Hindawi
Shock and Vibration
Volume 2019, Article ID 4652328, 12 pages
https://doi.org/10.1155/2019/4652328

Research Article

Impact of Damping Models in Damage Identification

Michael Souza,[1] **Daniel Castello**,[2] **Ney Roitman**,[1] **and Thiago Ritto**[2]

[1]*Department of Civil Engineering, Federal University of Rio de Janeiro, Rio de Janeiro, Brazil*
[2]*Department of Mechanical Engineering, Federal University of Rio de Janeiro, Rio de Janeiro, Brazil*

Correspondence should be addressed to Michael Souza; michael_leone@poli.ufrj.br

Received 20 November 2018; Revised 25 February 2019; Accepted 4 March 2019; Published 9 May 2019

Academic Editor: Filippo Ubertini

Several damage identification approaches are based on computational models, and their diagnostics depend on the set of modelling hypotheses adopted when building the model itself. Among these hypotheses, the choice of appropriate damping models seems to be one of the key issues. The goal of this paper is to analyze the impact of a set of damping models on the damage identification diagnostics. The damage identification is built on a Bayesian framework, and the measured data are the modal data associated with the first modes of the structure. The exploration of the posterior density of unknown model parameters is performed by means of the Markov chain Monte Carlo method (MCMC) with Delayed Rejection Adaptive Metropolis (DRAM) algorithm. The analyses are based on experimental dynamic response obtained from an aluminum beam instrumented with a set of accelerometers. The presence of damage/anomaly within the system is physically simulated by placing lumped masses over the beam, considering three different masses and two different placing positions. For the set of cases analyzed, it is shown that the proposed approach was able to identify both the position and magnitude of the lumped masses and that the damping models may not provide an increase of knowledge of some unknown parameters when damping rates are lower than 1%.

1. Introduction

Computational models were introduced in science and engineering in order to simulate the behavior of physical systems [1]. A key aspect for these analyses is the reliability of the predictions provided by computational models. In general, it is not straightforward to ensure the compliance with the real system due to the great number of unknowns and uncertainties related to material and physical properties, boundary conditions, load conditions, etc. [2]. Hence, one usually adopts simplifying hypotheses which may detract the quality and accuracy of the predictions provided by the model.

These issues had led to the development of model updating techniques [3] which aims to estimate unknown system parameters conjugating model structures, measured data, and optimization strategies. One specific framework that deserves attention is the Bayesian FE model updating methods which are based on Bayes' theorem [4]. The Bayesian framework provides means to obtain information about unknown model parameters as well as their uncertainties; moreover, its output can be used for uncertainty quantification analysis, global sensitivity analysis [5], and risk assessments, to cite a few. The number of applications of Bayesian FE model updating in the structural dynamics field has increased in the last decades. The review paper by Huang et al. [6] presents a comprehensive material concerning Bayesian inference in structural system identification on both vibration and wave propagation analyses. Katafygiotis and Beck [7] addressed the problem of updating a structural model and its associated uncertainties. Beck [8] used the Bayes' theorem to update the relative plausibility of candidate models within a set of model classes considering measured data and an initial plausibility of each model. As for its implementation, it should be highlighted that the Bayesian analyses depend on pseudorandom samples generation techniques and acceptance rejection procedures of candidate model parameters. In this context, Nicholas

Metropolis and coworkers presented the main background for statistical inference [9–11]. Finally, theoretical aspects can be found in the reference works in [12–15].

One of the many applications of Bayesian framework on civil and mechanical engineering is for structural health monitoring (SHM) [6, 16]. It is based on the premise that damaged structures will significantly modify their stiffness, mass, or energy dissipation properties, which, in turn, will change the measured dynamic response of the system [16]. In this context, it is imperative to fully understand the role of each hypothesis on the dynamical behavior of the structures under analysis. As for damping modelling, one may cite some important aspects to discuss, such as: Which is the best damping model to be used? Once one has obtained damping characteristics of the healthy structure, should one change the damping model when the structure gets damaged? What if one simply ignores damping models? The answer of these complex questions involves structural and material damping formulation. As for damping and damage, Bovsunovsky and Surace [17] studied the influence of damping levels on the nonlinear dynamic behavior of a component in order to assess crack's parameters; Chandra et al. [18] presented the state of the art of research on damping in fiber-reinforced composite materials and structures with emphasis on polymer composites. Prediction analyses of an anisotropic-damping matrix of a composite material were published in [19]. Gibson and Plunkett [20] described the analytical and experimental internal damping and elastic stiffness of E-glass fiber-reinforced epoxy beams under flexural vibration, and Ling and Haldar [21] proposed a novel system identification that could consider both viscous and Rayleigh-type proportional damping in dynamic models.

The objective of this paper is to analyze the impact of damping model choices on damage identification. Four damping models commonly used by the structural engineering community were considered. The damage scenarios are physically simulated as system anomalies which in the present work correspond to the placement of rigid blocks over an elastic beam. The identification is phrased as a statistical inverse problem using the Bayesian framework. The exploration of the posterior probability density function (pdf) of the unknown parameters is performed by means of the Markov chain Monte Carlo method (MCMC) with Delayed Rejection Adaptive Metropolis (DRAM) algorithm [22].

2. Theoretical Approach

The governing equation of an n DOF dynamic system is generally written as follows:

$$\mathbf{M}\ddot{\mathbf{u}}(t) = g(\mathbf{u}(t), \dot{\mathbf{u}}(t)) + \mathbf{F}(t), \tag{1}$$

where $\mathbf{M} \in \mathbb{R}^{n\times n}$ is the mass matrix of the system, $\mathbf{F}(t) \in \mathbb{R}^n$ is the vector containing the forces external to the system, $\mathbf{u} \in \mathbb{R}^n$ is the vector describing the system configuration, and the dot over a variable denotes its time derivative. As for the operator $g(\mathbf{u}(t), \dot{\mathbf{u}}(t))$, it is in charge of describing the relation between $\mathbf{u}$ and the restoration forces, as well as the relation between $(\mathbf{u}(t), \dot{\mathbf{u}}(t))$ and the dissipation forces. When the system is linear, the restoration force is described as a function of the stiffness matrix $\mathbf{K} \in \mathbb{R}^{n\times n}$ and it is equal to $(-1)\mathbf{Ku}$. As for the dissipation forces, among some possibilities, in this paper, they are restricted to the class: (i) which may be properly described as being viscous and (ii) which solely depends on the velocity at the current instant of time t, i.e., $\dot{\mathbf{u}}(t)$. These simplifications allow one to rewrite the governing equation (2) [23, 24] as follows:

$$\mathbf{M}\ddot{\mathbf{u}}(t) + \mathbf{D}\dot{\mathbf{u}}(t) + \mathbf{K}\mathbf{u}(t) = \mathbf{F}(t), \tag{2}$$

where $\mathbf{D} \in \mathbb{R}^{n\times n}$ is the viscous damping matrix. The matrix $\mathbf{D}$ should be positive definite such that the power produced by the dissipative force is always negative, i.e., $(-1)\mathbf{D}\dot{\mathbf{u}} \cdot \dot{\mathbf{u}} < 0$ for all $\dot{\mathbf{u}} \neq 0$.

There are basically two ways to define the matrix $\mathbf{D}$. The first one appears as the natural result of hypotheses that were adopted when writing the governing equations in the continuum. The second way is simply to adopt an ad hoc choice. As for the ad hoc choices, the ones which allow the diagonalization of the matrix $\mathbf{D}$ by the undamped mode shape matrix $\mathbf{\Phi}$ are particularly compelling due to the fact that they are prone to analytical treatment in some sense. One may cite, for example, the choice named proportional damping matrix [24], which is described as follows:

$$\mathbf{D} = \alpha\mathbf{M} + \beta\mathbf{K}, \tag{3}$$

where $\alpha \in \mathbb{R}^+$ and $\beta \in \mathbb{R}^+$ are user defined. The damping matrix in equation (3) can be diagonalized by the undamped mode shape matrix $\mathbf{\Phi}$.

One key aspect here is the fact that it does not matter if one builds the viscous damping matrix $\mathbf{D}$ by means of constitutive equations starting from the continuum or by an ad hoc choice; the user still has to determine the physical parameters or ad hoc parameters that characterize the matrix $\mathbf{D}$. At this point, any choice associated to the matrix $\mathbf{D}$ will have an impact on the model predictions provided by equation (2) and consequently on any identification strategy based on this model. Moreover, it is also true for any model-based damage identification approach.

The structure analyzed in this paper is an aluminum beam, and it will be presented in detail in Section 4. Nevertheless, in order to present which damping models will be treated here, it is necessary to give some information about the identification problem at this point. The present damage identification is rephrased as the quest for information about system anomalies placed over an elastic beam. The anomaly itself is a rigid block whose model parameterization is given by its location X_m over the beam and by its mass magnitude M_m. Therefore, concerning the identification process based on equation (2), the computational model will be described by a set of known model parameters and by a set of unknown model parameters that will be the components of the unknown vector $\boldsymbol{\theta} \in \mathbb{R}^{N_\theta}$.

The parameters X_m and M_m are of main interest for the identification in this work and are present in the unknown vector $\boldsymbol{\theta}$. Nevertheless, it should be emphasized that beyond X_m and M_m, some other parameters may possibly be additional components of $\boldsymbol{\theta}$. In the present work, these

additional components will be dependent on the damping model that is adopted when performing the system identification procedures. The damping models are options that are commonly used by the structural engineering community. Next, four damping model hypotheses and the corresponding unknown vector $\boldsymbol{\theta}$ that is associated with each hypothesis are described.

(i) Damping hypothesis 1 (DH1): the system is undamped. Thus, $\boldsymbol{\theta} = \{E, X_{\mathrm{m}}, M_{\mathrm{m}}\}^{\mathrm{T}}$, where E is Young's modulus and X_{m} and M_{m} are, respectively, the position and magnitude of structural anomaly.

(ii) Damping hypothesis 2 (DH2): the system is governed by Rayleigh's proportional damping model. Thus, $\boldsymbol{\theta} = \{E, \alpha, \beta, X_{\mathrm{m}}, M_{\mathrm{m}}\}^{\mathrm{T}}$, where α and β are the damping coefficients of the model shown in equation (3).

(iii) Damping hypothesis 3 (DH3): the system is governed by Rayleigh's proportional damping model shown in equation (3). Nevertheless, in this case, the damping coefficients are considered equal to the ones that were estimated for the healthy/intact structure [25]. Thus, $\boldsymbol{\theta} = \{E, X_{\mathrm{m}}, M_{\mathrm{m}}\}^{\mathrm{T}}$.

(iv) Damping hypothesis 4 (DH4): the system is governed by a damping model which provides the same damping ratio ζ^* for all modes. In this case, we also have $\boldsymbol{\theta} = \{E, X_{\mathrm{m}}, M_{\mathrm{m}}\}^{\mathrm{T}}$.

Two points should be emphasized at this point. The first one is that, in this study, it is considered that Young's modulus E is also a component of the unknown vector $\boldsymbol{\theta}$. Nevertheless, its range of variation is restricted to a tight region. Therefore, it is used here to compensate for possible uncertainties in its nominal value. The second one is concerned with the damping matrix of the fourth damping hypothesis (DH4). It is built as follows:

$$\mathbf{D} = \left[\boldsymbol{\Phi}^{-1}\right]^{\mathrm{T}} 2\left(\zeta^* \mathbf{I}_{n\times n}\right)\boldsymbol{\Omega}\left[\boldsymbol{\Phi}^{-1}\right], \tag{4}$$

where $\zeta^* \in \mathbb{R}^+$ is the damping rate chosen by the user, $\mathbf{I}_{n\times n}$ is the identity matrix, and $\boldsymbol{\Omega}$ is a diagonal matrix containing the undamped natural frequencies of the system, i.e., $[\boldsymbol{\Omega}]_{\mathrm{pq}} = \omega_{\mathrm{p}}\delta_{\mathrm{pq}}$. A key aspect in this case is that, the user may model ζ^* as a random variable chosen from a uniform distribution defined between the minimum experimental value of damping rate and its maximum experimental value, i.e., $\zeta^* \sim \mathcal{U}(\min(\zeta_k^{\mathrm{exp}}), \max(\zeta_k^{\mathrm{exp}}))$ where k represents the k-th vibration mode of interest.

Finally, it should be highlighted that the damping models adopted are amenable for structural damping and they are not meant to describe localized damping mechanisms such as the ones one may observe when facing cracks, for example. Specific information concerning cracks and damping could be found in [26].

3. Bayesian Framework

3.1. Classical Approach. In a Bayesian framework, all unknown quantities and measurements are modeled as random variables, where the uncertainties related to each parameter are described by their probability density functions [14]. Henceforward, the following notation is used for this framework: $\pi(\boldsymbol{\theta})$ denotes the probability density function (pdf) of a random variable θ, $\pi(\boldsymbol{\theta}, r)$ defines the joint probability of the random variables θ and r, $\pi(\boldsymbol{\theta} \mid r)$ denotes the conditional probability of θ given r, and $\pi(\boldsymbol{\theta})$ denotes the pdf of a random vector $\boldsymbol{\theta}$.

Consider that one may measure a set of output variables from the system $\mathbb{S}$ and organize them in a column vector $\mathbf{y} \in \mathbb{R}^{N_y}$. The measurements in $\mathbf{y}$ are often quantities that are of interest for control, identification, and model calibration such as displacements, strains, forces, and modal data, to cite a few. In general terms, the connection between the model prediction $\mathbf{y}^{\mathrm{m}}$ and the corresponding measurements $\mathbf{y}$ is given by an additive error observation model [1, 14]:

$$\mathbf{y} = \mathbf{G}(\boldsymbol{\theta}) + \mathbf{e}, \tag{5}$$

where $\mathbf{G}(\boldsymbol{\theta}) = \mathbf{y}^{\mathrm{m}}$ is an operator that provides model predictions for the same quantities that were measured in $\mathbf{y}$. As for $\boldsymbol{\theta} \in \mathbb{R}^{N_\theta}$, it denotes the random vector of the unknown parameters of the system $\mathbb{S}$ and, in the present formulation, they depend on the damping model adopted along the damage identification process as described in Section 2. Finally, it is assumed that the model described by the operator $\mathbf{G}(\boldsymbol{\theta})$ is accurate and that the discrepancies between measurements $\mathbf{y}$ and model predictions $\mathbf{G}(\boldsymbol{\theta}) = \mathbf{y}^{\mathrm{m}}$ may be properly described by the random variable $\mathbf{e} \in \mathbb{R}^{N_y}$ which is in charge of describing the measurement errors and whose probability density functions is given by $\pi_e(\mathbf{e})$.

As $\mathbf{y}$, $\mathbf{e}$, and $\boldsymbol{\theta}$ are random variables or vectors, the Bayes rule [14] may be used to connect the information among them as follows:

$$\pi(\boldsymbol{\theta} \mid \mathbf{y}) = \frac{\pi(\mathbf{y} \mid \boldsymbol{\theta})\pi_{\mathrm{PR}}(\boldsymbol{\theta})}{\pi(\mathbf{y})}, \tag{6}$$

where $\pi(\boldsymbol{\theta} \mid \mathbf{y})$ is the posterior probability density function, $\pi(\mathbf{y} \mid \boldsymbol{\theta})$ is the likelihood function, $\pi_{\mathrm{PR}}(\boldsymbol{\theta})$ is the prior pdf, and $\pi(\mathbf{y})$ is the density of measured data. The posterior density $\pi(\boldsymbol{\theta} \mid \mathbf{y})$ is the main objective of the Bayesian inverse problem. The prior pdf contains our current state of knowledge about the uncertainty model parameters $\boldsymbol{\theta}$.

Assuming that the model parameters $\boldsymbol{\theta}$ and the additive noise vector $\mathbf{e}$ are mutually independent, the likelihood function is given by $\pi(\mathbf{y} \mid \boldsymbol{\theta}) = \pi_{\mathrm{e}}(\mathbf{y} - \mathbf{G}(\boldsymbol{\theta}))$ [14], in which $\pi_r(q)$ denotes the pdf of the random variable r evaluated at the argument $r = q$. In other words, this gives the probability of observing measured data $\mathbf{y}$, given a set of parameters $\boldsymbol{\theta}$ for the model. As for the density $\pi(\mathbf{y})$, it is hardly available inasmuch as it would require a large number of experimental tests. Fortunately, it acts as a scaling factor and it is of little importance when using sample-based techniques to explore the posterior $\pi(\boldsymbol{\theta} \mid \mathbf{y})$ [5, 14, 27].

The complete probabilistic approach for model updating structural anomalies is presented in equation (6). Therefore, one can compute various point estimates for the random vector $\boldsymbol{\theta}$ along with *a posteriori* uncertainties for these estimates after obtaining the posterior distribution $\pi(\boldsymbol{\theta} \mid \mathbf{y})$. There are several point estimates that can be computed such as the ones shown as follows:

$$\mathbb{E}_{\theta|\mathbf{y}}(\boldsymbol{\theta}) = \int_{\mathscr{D}_\theta} \boldsymbol{\theta}\pi(\boldsymbol{\theta}\,|\,\mathbf{y})d\boldsymbol{\theta},$$
$$\widehat{\boldsymbol{\theta}}_{\mathrm{MAP}} = \arg\max_{\boldsymbol{\theta}\in\mathscr{D}_\theta} \pi(\boldsymbol{\theta}\,|\,\mathbf{y}), \tag{7}$$
$$\widehat{\boldsymbol{\theta}}_{\mathrm{ML}} = \arg\max_{\boldsymbol{\theta}\in\mathscr{D}_\theta} \pi(\mathbf{y}\,|\,\boldsymbol{\theta}),$$

where $\mathbb{E}_{\theta|\mathbf{y}}(\boldsymbol{\theta})$ represents the expected value, $\widehat{\boldsymbol{\theta}}_{\mathrm{MAP}}$ defines the maximum *a posteriori* estimator (MAP), $\widehat{\boldsymbol{\theta}}_{\mathrm{ML}}$ denotes the maximum likelihood estimator (ML), and $\mathscr{D}_{(\bullet)}$ defines the domain of the random variable, or vector, of interest.

It should be noted that integrals like the ones presented in equation (7) are quite common when dealing with statistical inverse problems [14] and uncertainty quantification analysis [5]. Moreover, they generally do not have analytical solutions because the operator $\mathbf{G}(\boldsymbol{\theta})$ generally involves a nonlinear map between the unknown random vector $\boldsymbol{\theta} \in \mathbb{R}^{N_\theta}$ and the model predictions $\mathbf{G}(\boldsymbol{\theta}) \in \mathbb{R}^{N_y}$. Therefore, one usually resorts to Markov chain Monte Carlo methods to extract information from the posterior density.

A MCMC method is any method that allows one to draw samples $\{\boldsymbol{\theta}^{(1)}, \ldots, \boldsymbol{\theta}^{(\mathrm{mc})}\}$ to simulate a target density $\overline{\pi}(\boldsymbol{\theta})$. In this work, the DRAM algorithm is used to generate samples from the posterior density $\pi(\boldsymbol{\theta}\,|\,\mathbf{y})$.

3.2. DRAM Algorithm. DRAM is an algorithm proposed by Haario et al. [22] that aims at improving the efficiency of the MCMC, using concepts of the Delayed Rejection (DR) and Adaptive Metropolis (AM). As earlier stressed, a MCMC is any method that produces drawn samples (states) $\{\boldsymbol{\theta}^{(1)}, \ldots, \boldsymbol{\theta}^{(\mathrm{mc})}\}$ from a target probability density function $\overline{\pi}(\boldsymbol{\theta})$ [27]. This method often allows drawing samples such that the actual state, i.e., $\boldsymbol{\theta}^{(t)}$, depends solely on the previous state $\boldsymbol{\theta}^{(t-1)}$. There are several MCMC methods, for example, the Metropolis (M) algorithm [11], the Metropolis–Hastings (MH) [10], and the Gibbs sampler (GS) [28], to cite a few.

The basic concepts of the DRAM algorithm are the adaptive Metropolis (AM), which is addressed to adapt the proposal distribution based on the past history of the draws that have already been accepted in the actual Markov Chain, and the Delayed Rejection (DR), which is a strategy to modify the classical MH algorithm to improve its efficiency of the resulting MCMC estimates relative to asymptotic variance ordering. Thus the Delayed Rejection Adaptive Metropolis (DRAM) takes the main characteristics of DR and AM in order to improve the acceptance ratio, which leads to a reduction of the computational cost to properly explore the target density $\overline{\pi}(\boldsymbol{\theta})$.

In a classic Metropolis–Hastings approach, a new candidate $\boldsymbol{\theta}^{(c)}$ is generated from a proposal distribution q_1 and its acceptance depends on the MH-acceptance ratio $\alpha_{\mathrm{MH}}^{(1)}$ shown as follows:

$$\alpha_{\mathrm{MH}}^{(1)}\left(\boldsymbol{\theta}^{(\mathrm{c})}\,\middle|\,\boldsymbol{\theta}^{(t-1)}\right) = \min\left\{1, \frac{\overline{\pi}\left(\boldsymbol{\theta}^{(\mathrm{c})}\right) q_1\left(\boldsymbol{\theta}^{(\mathrm{c})}\,\middle|\,\boldsymbol{\theta}^{(t-1)}\right)}{\overline{\pi}\left(\boldsymbol{\theta}^{(t-1)}\right) q_1\left(\boldsymbol{\theta}^{(t-1)}\,\middle|\,\boldsymbol{\theta}^{(\mathrm{c})}\right)}\right\}$$
$$= \min\left\{1, \frac{N_1}{D_1}\right\}. \tag{8}$$

Upon rejection, instead of keeping the chain at the state $(t-1)$, a second candidate $\boldsymbol{\theta}^{(c,2)}$ is proposed. A second proposal, q_2, depends not only on the current position $\boldsymbol{\theta}^{(t-1)}$ of the chain but also on what one has just proposed and rejected $\boldsymbol{\theta}^{(c)}$. The probability of acceptance depends on the updated MH-acceptance ratio $\alpha_{\mathrm{MH}}^{(2)}$ which is ruled by equation (9). The methodology of DR can be expanded for an arbitrary number of stages working on an iterative process. Figure 1 presents a prompt but illustrative sketch of the Delayed Rejection step in the perspective of DRAM algorithm.

$$\alpha_{\mathrm{MH}}^{(2)}\left(\boldsymbol{\theta}^{(\mathrm{c},2)}\,\middle|\,\boldsymbol{\theta}^{(\mathrm{c})}, \boldsymbol{\theta}^{(t-1)}\right) = \min\left\{1, \frac{\overline{\pi}\left(\boldsymbol{\theta}^{(\mathrm{c},2)}\right) q_1\left(\boldsymbol{\theta}^{(\mathrm{c})}\,\middle|\,\boldsymbol{\theta}^{(t-1)}\right) q_2\left(\boldsymbol{\theta}^{(\mathrm{c},2)}\,\middle|\,\boldsymbol{\theta}^{(\mathrm{c})}, \boldsymbol{\theta}^{(t-1)}\right)\left[1-\alpha_1\left(\boldsymbol{\theta}^{(\mathrm{c})}\,\middle|\,\boldsymbol{\theta}^{(t-1)}\right)\right]}{\overline{\pi}\left(\boldsymbol{\theta}^{(t-1)}\right) q_1\left(\boldsymbol{\theta}^{(t-1)}\,\middle|\,\boldsymbol{\theta}^{(\mathrm{c})}\right) q_2\left(\boldsymbol{\theta}^{(t-1)}\,\middle|\,\boldsymbol{\theta}^{(\mathrm{c},2)}, \boldsymbol{\theta}^{(\mathrm{c})}\right)\left[1-\alpha_1\left(\boldsymbol{\theta}^{(t-1)}\,\middle|\,\boldsymbol{\theta}^{(\mathrm{c})}\right)\right]}\right\} = \min\left\{1, \frac{N_2}{D_2}\right\}. \tag{9}$$

As for the adaptive Metropolis, the basic idea of AM is to calibrate the covariance matrix of the proposal distribution, e.g., the normal distribution, using the sample path of the MCMC, i.e., the past states of the chain. The process starts from an initial covariance matrix $\sum^{(0)}$, and the covariance of the proposal pdf is updated at arbitrary intervals according to the rule given by equation (10).

$$\sum^{(t)} = \left(\mathrm{Cov}\left(\boldsymbol{\theta}^{(t-k)}, \ldots, \boldsymbol{\theta}^{(t-1)}, \boldsymbol{\theta}^{(t)}\right) + \mathbf{I}_n\eta\right)s, \tag{10}$$

where $\mathbf{I}_n$ represents the n-dimensional identity matrix, η is a small number used to prevent that the updated covariance matrix $\sum^{(t)}$ becomes singular, and s is a scaling factor. Further details from this algorithm may be found in [22].

4. Experimental Setup

A simply supported aluminum beam was taken to perform experimental analyses. The beam's physical properties are length $L = 1464$ mm; rectangular cross section with width $b = 76.2$ mm, height $h = 6$ mm, and mass density $\rho = 2700$ kg/m^3. Figure 2 shows the experimental setup.

The experimental setup is composed of accelerometers; PCB Piezotronics models 336C and 336C31, used in this modal analysis to collect the acceleration responses of the

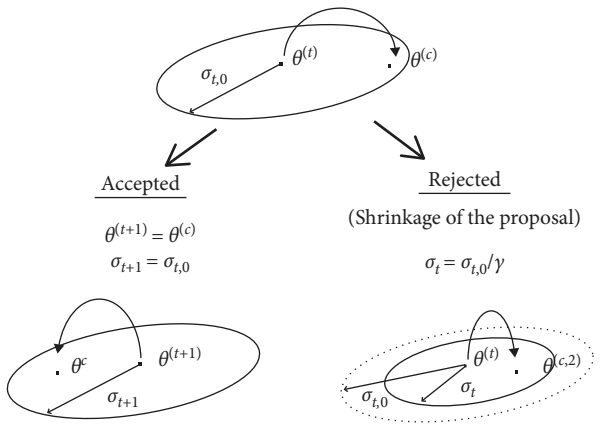

Figure 1: Delayed rejection illustrative sketch for a generic random variable ($\sigma_{t,0}$ illustrates the variance of the random walk at an initial stage).

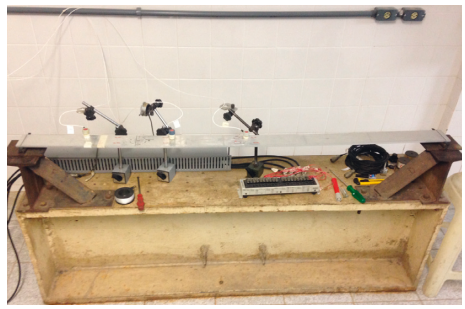

Figure 2: Experimental setup.

structure at three different positions; an impact hammer, model 086C01 PCB Piezotronics to provide excitation; the acquisition system is formed by model 481 PCB Piezotronics signal conditioner; and model APS2000 data acquisition manufactured by Lynx Tecnologia. The accelerometers were placed in order to record until the fifth vibration mode. Their masses were measured and added into the numerical model.

In this research, the structural anomalies were simulated by the addition of masses at two specific sections of the structure. In order to analyze different magnitudes of structural anomalies, four punctual masses were adopted as detailed in Figure 3. The dimensions of the rigid blocks were taken into consideration when building the computational model of the system.

A SIMO analysis (single input multiple output) was performed for each structural anomaly scenario detailed in Table 1. The dynamic loads were provided by twenty impacts of the hammer with thirty seconds mean gap. The measuring frequency range was set as 0–250 Hz, and the signal was low-pass filtered with a cutoff frequency of 250 Hz. The data acquisition frequency was set to 1000 Hz.

Figure 4 shows an illustration of the accelerometers positions, impact positions as well as the Sections S1 and S2 where the rigid blocks were placed in order to simulate structural anomalies.

The vibration data was postprocessed by an in-house program which yields an estimation of damping ratios and

Figure 3: Magnitudes of lumped masses: 158.4 g; 94.5 g; 49.6 g; and 36.9 g, respectively.

Table 1: Structural anomalies scenarios.

Anomaly index	Added mass	Position	Section
A1	158.4 g	300 mm	S1
A2	49.6 g	300 mm	S1
A3	94.5 g	859 mm	S2
A4	36.9 g	859 mm	S2

natural frequencies. The program uses the Short Time Fourier-Transform (STFT) to infer about the modal properties and calculates the time-frequency distribution (TFDs) of the signal that contains the time domain response due to the impact. After choosing the vibration mode of interest, the modal damping factors are estimated by means of a linear regression of the vibration amplitude curve. This postprocessing procedure was repeated for all the twenty impacts of the hammer for the first five vibration modes for each one of the anomaly scenarios that were considered. The experimental data vector was estimated by the expected value of natural frequencies and damping rates. In this paper, the standard deviation was used as the estimator of the uncertainties related to these dynamic properties. Twenty samples of each modal data were collected, as detailed in Tables 2 and 3 where μ_k and σ_k denote the empirical mean and the empirical standard deviation of the variable k.

5. Results and Discussion

The results and assessments of the proposed approach using measured data are presented in this section. Model updating for structural anomaly and subsequent validation analyses are detailed as well as their corresponding discussions. The model updating for the healthy structure and the optimization values of anomaly scenarios are detailed in [25].

The experimental data used for Bayesian model updating comprise the natural frequencies and damping rates computed from accelerations measured by the accelerometers AC1, AC2, and AC3 when an impact force is applied to the structure. The dynamic analysis also provided the FRFs for all anomaly scenarios and accelerometer's positions. The computational models were validated by comparisons between the experimental FRFs and their computed counterparts at the accelerometer's position AC1 of anomaly scenarios A1 and A4. These two scenarios were chosen because they are the biggest and the lowest structural masses, respectively, i.e. the A1's magnitude is thereabout 8% of the beam's weight and A4's magnitude is nearly 2%.

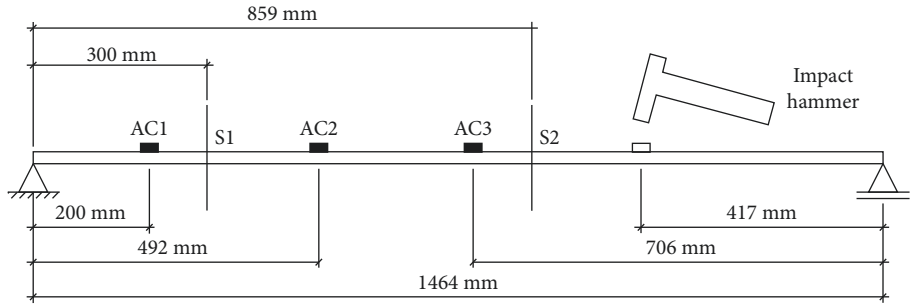

Figure 4: Illustrative sketch of accelerometers AC1, AC2, and AC3 and impact hammer positions along the structure.

Table 2: Experimental modal results for A1 and A2 configurations (damping rates (10^{-2})).

Mode	μ_ω (Hz)	σ_ω (Hz)	μ_ζ (%)	σ_ζ (%)
A1				
1st	6.59	0.01	40.39	0.33
2nd	25.19	0.01	26.24	0.30
3rd	57.16	0.03	36.74	0.50
4th	104.32	0.14	79.97	3.85
5th	165.25	0.23	122.02	9.79
A2				
1st	6.71	0.01	37.98	0.23
2nd	26.31	0.01	23.09	0.45
3rd	59.14	0.02	28.28	0.60
4th	105.21	0.09	64.79	3.16
5th	165.78	0.05	43.58	2.21

Table 3: Experimental modal results for A3 and A4 configurations (damping rates (10^{-2})).

Mode	μ_ω (Hz)	σ_ω (Hz)	μ_ζ (%)	σ_ζ (%)
A3				
1st	6.50	0.01	40.09	0.23
2nd	26.57	0.01	21.76	0.24
3rd	59.16	0.02	31.78	1.01
4th	102.61	0.11	66.6	3.43
5th	165.46	0.39	45.07	2.85
A4				
1st	6.66	0.01	38.46	0.23
2nd	26.76	0.01	20.89	0.18
3rd	59.84	0.02	31.73	1.95
4th	104.48	0.18	62.49	4.31
5th	165.87	0.08	41.74	2.84

The computational model is based on the finite element method (FEM), with 15 elements, considering the Euler–Bernoulli beam's hypothesis. The model updating is driven by the hypothesis that the anomaly does not influence the stiffness of the elements. The local mass matrices are calculated as follows [23].

$$\mathbf{M}^{\mathrm{e}} = \int_{\Omega_e} \rho(x)\mathbf{N}(x)\mathbf{N}(x)^{\mathrm{T}}\,dx,$$

$$\rho(x) = \begin{cases} \rho_{\mathrm{b}}, & 0 < x < X_{\mathrm{m}} - \dfrac{l_{\mathrm{m}}}{2}, \\ & X_{\mathrm{m}} + \dfrac{l_{\mathrm{m}}}{2} < x < l_{\mathrm{e}}, \\ \rho_{\mathrm{b}} + \dfrac{M_{\mathrm{m}}}{l_{\mathrm{m}}}, & X_{\mathrm{m}} - \dfrac{l_{\mathrm{m}}}{2} < x < X_{\mathrm{m}} + \dfrac{l_{\mathrm{m}}}{2}, \end{cases} \tag{11}$$

where $\mathbf{M}^{\mathrm{e}}$ is the element mass matrix, $\mathbf{N}(x)$ is the matrix containing the shape functions, $\rho(x)$ is the linear specific mass of the structure, ρ_{b} is the linear specific mass of the beam, l_{m} is the width of the rigid block, l_{e} is the length of the element, and M_{m} is the mass of the rigid block.

5.1. Bayesian Inference Remarks. The Bayesian inference analysis requires one to specify the likelihood $\pi(\mathbf{y} \mid \boldsymbol{\theta})$ and the prior $\pi_{\mathrm{PR}}(\boldsymbol{\theta})$ in equation (6). As the likelihood function $\pi(\mathbf{y} \mid \boldsymbol{\theta})$ is defined by the distribution of the additive error, i.e., $\pi(\mathbf{y} \mid \boldsymbol{\theta}) = \pi_{\mathrm{e}}(\mathbf{y} - \mathbf{G}(\boldsymbol{\theta}))$, whereupon in this study it was adopted the common choice $\mathbf{e} \sim N(\mathbf{0}, \sum_{\mathrm{e}})$. This demands the specification of the covariance matrix $\sum_{\mathrm{e}}$. As for the impact of likelihood distribution on Bayesian model updating, Souza [25] compared two hypotheses for $\sum_{\mathrm{e}}$ to be used in a damping model calibration process using data from the present aluminum beam, namely, full-empirical covariance matrix and diagonal empirical covariance matrix. They demonstrated that both hypotheses led to the same predictions approximately. Therefore, for the present analyses, a diagonal empirical covariance matrix $\sum_{\mathrm{e}}$ that was built with measured data extracted from Tables 2 and 3 was assumed.

As for the priors, they were built as follows. Firstly, a deterministic analysis was performed in order to identify the maximum likelihood estimate $\widehat{\boldsymbol{\theta}}_{\mathrm{ML}}$ described in equation (7). The *approximate* posterior covariance matrix is then computed as $\widehat{\sum}_\theta \approx (\mathbf{J}^{\mathrm{T}} \sum_{\mathrm{e}} \mathbf{J})^{-1}$ [1] in which the operator $\mathbf{J}$ corresponds to the model Jacobian evaluated at $\widehat{\boldsymbol{\theta}}_{\mathrm{ML}}$. Secondly, we assume the prior as follows: $\pi_{\mathrm{PR}}(\boldsymbol{\theta}) \sim N(\widehat{\boldsymbol{\theta}}_{\mathrm{ML}}, \Gamma)$, where Γ is a diagonal matrix whose r-th diagonal component is given as $\Gamma_{\mathrm{rr}} = \sigma_r^2 = \lambda^2 (\widehat{\Sigma}_\theta)_{\mathrm{rr}} = \lambda^2 \widehat{\sigma}_r^2$. Two different priors were considered, one for which $\lambda = 2$ and other $\lambda = 5$. Finally, samples $\left\{\boldsymbol{\theta}^{(1)}, \ldots, \boldsymbol{\theta}^{(N_{\mathrm{mc}})}\right\}$ from the posterior $\pi(\boldsymbol{\theta} \mid \mathbf{y})$ have been obtained with DRAM sampling algorithm [22]. $N_{\mathrm{mc}} = 20,000$ samples was considered.

The MCMC chain convergence was tested for the last 12,000 samples. The analyses of the cumulative mean and cumulative variance were adopted for assessing the stationarity of the posterior probability density function $\pi(\boldsymbol{\theta} \mid \mathbf{y})$.

After discarding the burn-in period, in order to perform the Geweke test [29], the MCMC chain has been split into several parts. We picked the first 10% and the last 50% of the chain and compared their means and variances. The chain was considered at its stationary configuration when the discrepancy between each moment was lower than 5%. Otherwise, a new burn-in period would be chosen and the test repeated until it complies with the Geweke criterion.

One strategy adopted for reducing autocorrelation was thinning the output by storing only at every 2 points after the burn-in period. Each MCMC sample's chain was evaluated by means of its autocorrelation. The results were low correlated, below 10% correlation for the first and last 1000 draws. The scatter plot of the position and magnitude of each anomaly scenario was analyzed in order to assess some level of sampling correlation.

A key aspect to build the prior statistical model is that every random variable, e.g., Young's modulus E, the position X_{m}, and magnitude M_{m} of punctual masses, and so forth, was constructed under the hypothesis that they are mutually independent [30]. Therefore, the prior joint density can be computed by the multiplication of the marginal densities. Moreover, the marginal prior for the variable r is defined to be within the set $\mathscr{D}_r$ as follows:

$$\begin{aligned}
\mathscr{D}_E &= \{E \in \mathbb{R} \mid 7 < E < 8, 2\}\left(10^{10}\ \mathrm{kPa}\right),\\
\mathscr{D}_\alpha &= \{\alpha \in \mathbb{R} \mid 2,5 < \alpha < 4\}\left(10^{-1}\ \mathrm{s}^{-1}\right),\\
\mathscr{D}_\beta &= \{\beta \in \mathbb{R} \mid 5,5 < \beta < 14\}\left(10^{-6}\ \mathrm{s}\right),\\
\mathscr{D}_{x_{\mathrm{m}}} &= \left\{X_{\mathrm{m}} \in \mathbb{R} \;\middle|\; 0 < X_{\mathrm{m}} < L\right\}(\mathrm{m}),\\
\mathscr{D}_{m_{\mathrm{m}}} &= \left\{M_{\mathrm{m}} \in \mathbb{R} \;\middle|\; 0 < M_{\mathrm{m}} < 0,5\right\}(\mathrm{kg}).
\end{aligned} \tag{12}$$

In order to quantify the influence of the damping models on the system identification, some results will be described by means of the scaled variables $X_{\mathrm{e}} = (X_{\mathrm{m}}/X_{\mathrm{true}})$ and $M_{\mathrm{e}} = (M_{\mathrm{m}}/M_{\mathrm{true}})$ based on the samples $\{X_{\mathrm{m}}^{(1)}, \ldots, X_{\mathrm{m}}^{(\mathrm{mc})}, M_{\mathrm{m}}^{(1)}, \ldots, M_{\mathrm{m}}^{(\mathrm{mc})}\}$ drawn from the posterior distribution.

To close up this section, we emphasize the Bayesian inference steps. Firstly, the DRAM algorithm was run and the burn-in period was removed from the samples of the MCMC chain. Secondly, the convergence analysis is performed where one verifies if the distribution has reached its stationary configuration and how its states are correlated. This step is crucial in the Bayesian inference because all the computational predictions come from the estimated posterior probability distribution. Finally, the postprocessing starts and we can infer about the position X_{m} and mass magnitude M_{m} of the rigid blocks under different scenarios. One could assess the influence of each damping model when analyzing the uncertainties encoded in the marginal densities $\pi(X_{\mathrm{m}} \mid \mathbf{y})$ and $\pi(M_{\mathrm{m}} \mid \mathbf{y})$.

5.2. Model Updating Results. Henceforth, for a given analysis, the generic notation DHiAj is used to denote the i-th damping model and the j-th anomaly configuration of interest. For example, DH2A4 denotes that the structure is governed by the Rayleigh proportional damping model and subjected to a structural anomaly simulated by a rigid block weighting $M_{\mathrm{m}} = 36.9$ g and located at $X_{\mathrm{m}} = 859$ mm along the beam length according to Table 1.

For all scenarios studied in this paper, the MCMC samples presented well-mixing chains with low correlated draws. Moreover, all the posterior distributions have reached their stationary configurations. In a general view, the MCMC chains stay below 10% correlation rates. It suggests that the DRAM algorithm could provide an unbiased picture of $\pi(\boldsymbol{\theta} \mid \mathbf{y})$. This conclusion is endorsed by the well-mixing samples. For example, Figure 5 shows the samples of position X_{m} and mass magnitude M_{m} for scenario DH1A1.

After convergence analyses have been performed, one may assess the main unknown variables of interest, i.e., position X_{m} and mass magnitude M_{m}. It means that, henceforth, information based on the marginal posterior densities $\pi(X_{\mathrm{m}} \mid \mathbf{y})$ and $\pi(M_{\mathrm{m}} \mid \mathbf{y})$ will be presented. Scatter plots were studied in an attempt to assess linear correlation between both parameters. Despite independence hypothesis adopted for all the uncertain variables in the prior density, the samples could still suggest some level of linear correlation due to the nonlinear mapping between the random vector $\boldsymbol{\theta}$ and the model predictions. The dispersion of variables was analyzed based on its scaled values $X_{\mathrm{e}} = (X_{\mathrm{m}}/X_{\mathrm{true}})$ and $M_{\mathrm{e}} = (M_{\mathrm{m}}/M_{\mathrm{true}})$. As earlier stated, this strategy provides a direct visualization of parameter deviation. Figure 6 shows the relationship between position X_{m} and magnitude M_{m} obtained in this paper. Moreover, it should be emphasized that the maximum deviations of X_{m}, around 10% and 20%, observed at samples drawn from prior covariance matrix with $\lambda = 2$, are quite low when compared with the deviations of X_{m} and M_{m} observed at samples drawn from prior covariance matrix with $\lambda = 5$. These results suggest that the positions have thinner pdfs when compared with the magnitude ones in the same anomaly scenario. This pattern can be better visualized in Figures 7–10.

Figures 7 and 9 present the scaled marginal posteriors of mass position X_{m} and magnitude M_{m} when the rigid blocks are located at Section S1, i.e., anomalies A1 and A2 in Table 1. Analogously, Figures 8 and 10 present the scaled marginal posteriors when the rigid blocks are located at Section S2, i.e., anomalies A3 and A4 in Table 1. It can be seen that independent of the anomaly scenario, the marginals $\pi(X_{\mathrm{m}} \mid \mathbf{y})$ present lower deviations than the marginals $\pi(M_{\mathrm{m}} \mid \mathbf{y})$. Preliminary sensitivity analyses indicated that X_{m} has greater influence on natural frequencies along the inference than the mass magnitudes M_{m}. On the other hand, both parameters did not suffer significant modifications as a function of the measured damping rates. Based on the fact that data vector $\mathbf{y}$ consists in natural frequencies and damping rates, the computational model will be more accurate for unknown parameters that provide the best compliance with the probabilistic model described in equation (6). In other words, as X_{m} ones have higher impact on the discrepancy $[\mathbf{y} - \mathbf{G}(\boldsymbol{\theta})]$ performed at $\pi(\mathbf{y} \mid \boldsymbol{\theta})$, the DRAM algorithm will be more selective to accept their candidate states when compared with M_{m} ones. This conclusion is endorsed when the shape of pdfs presented in Figures 7–10 are compared. These prompt evidences indicate

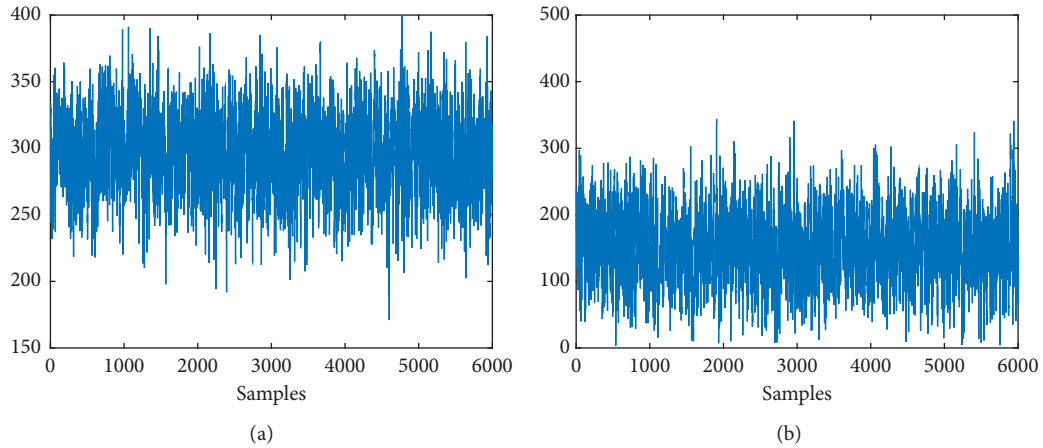

Figure 5: MCMC chain samples at DH1A1 for prior covariance matrix $\lambda = 2$. (a) Samples of X_m (mm). (b) Samples of M_m (g).

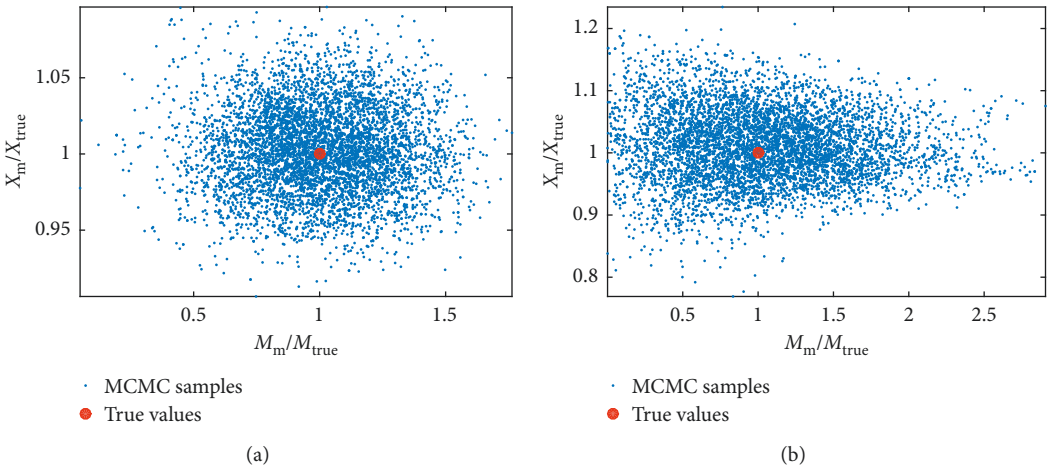

Figure 6: Scatter plot of the scaled $X_m \times M_m$ for DH2A3. (a) Prior covariance with $\lambda = 2$. (b) Prior covariance with $\lambda = 5$.

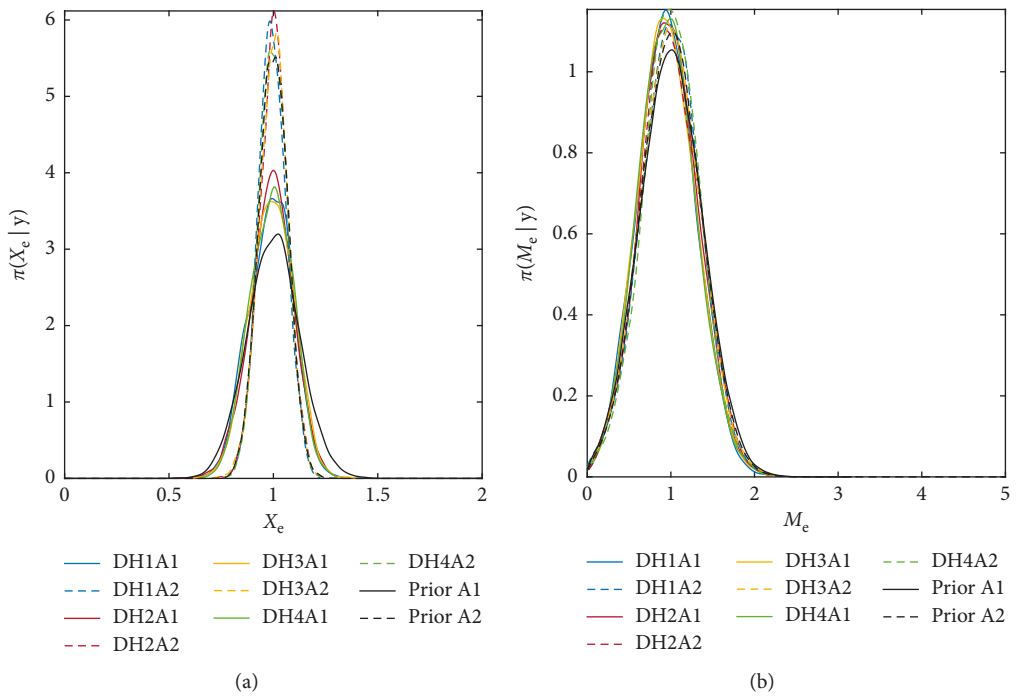

Figure 7: Anomaly scenarios A1 and A2. Prior covariance matrix with $\lambda = 2$. $X_e = (X_m/X_{true})$ and $M_e = (M_m/M_{true})$.

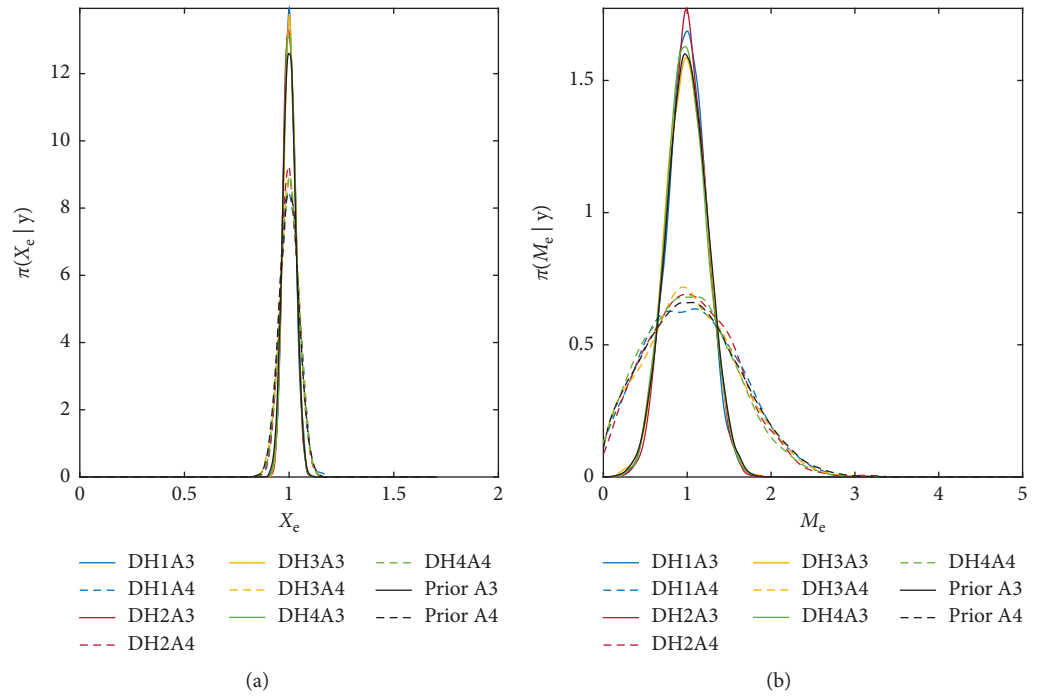

Figure 8: Anomaly scenarios A3 and A4. Prior covariance matrix with $\lambda = 2$. $X_e = (X_m/X_{true})$ and $M_e = (M_m/M_{true})$.

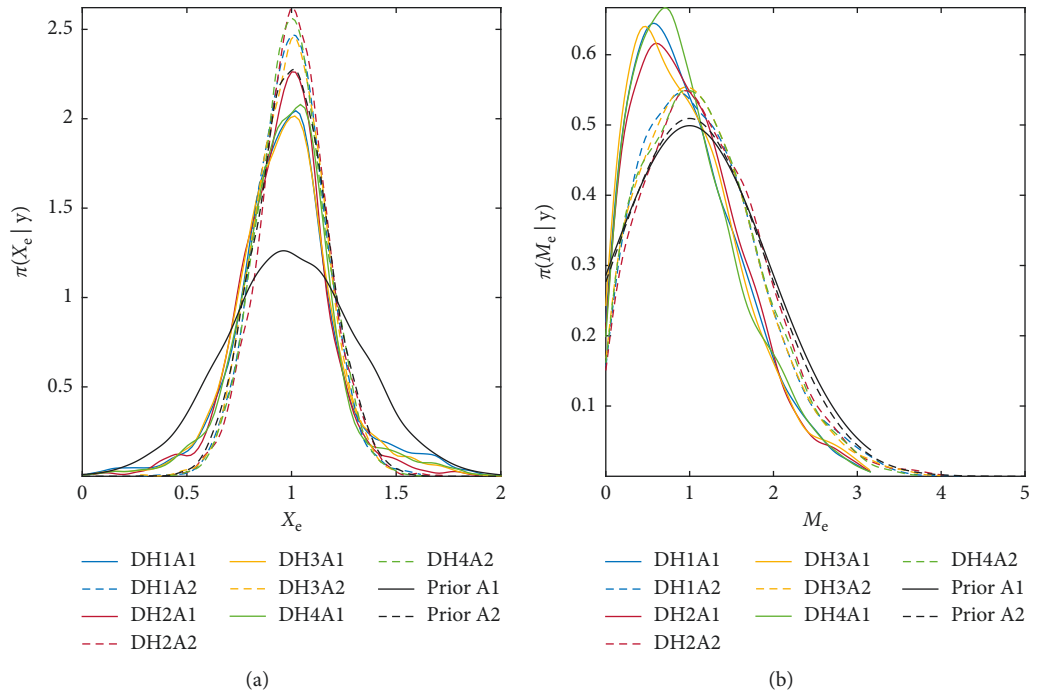

Figure 9: Anomaly scenarios A1 and A2. Prior covariance matrix with $\lambda = 5$. $X_e = (X_m/X_{true})$ and $M_e = (M_m/M_{true})$.

some path in order to fully understand the difference on the uncertainty level of both variable predictions X_m and M_m. However, the physical explanations for this were not fully explored and it is not the purpose of this paper.

In order to particularize the information of each unknown parameters prediction, Table 4 presents the mean and standard deviation of the priors $\pi(X_m)$ and $\pi(M_m)$ considering both situations $\lambda = 2$ and $\lambda = 5$ and Table 5 presents the same statistics for the marginal posteriors $\pi(X_m \mid \mathbf{y})$ and $\pi(M_m \mid \mathbf{y})$.

Further information may be extracted from Figures 7–10. The marginal densities $\pi(M_m \mid \mathbf{y})$ for scenarios DH1A3

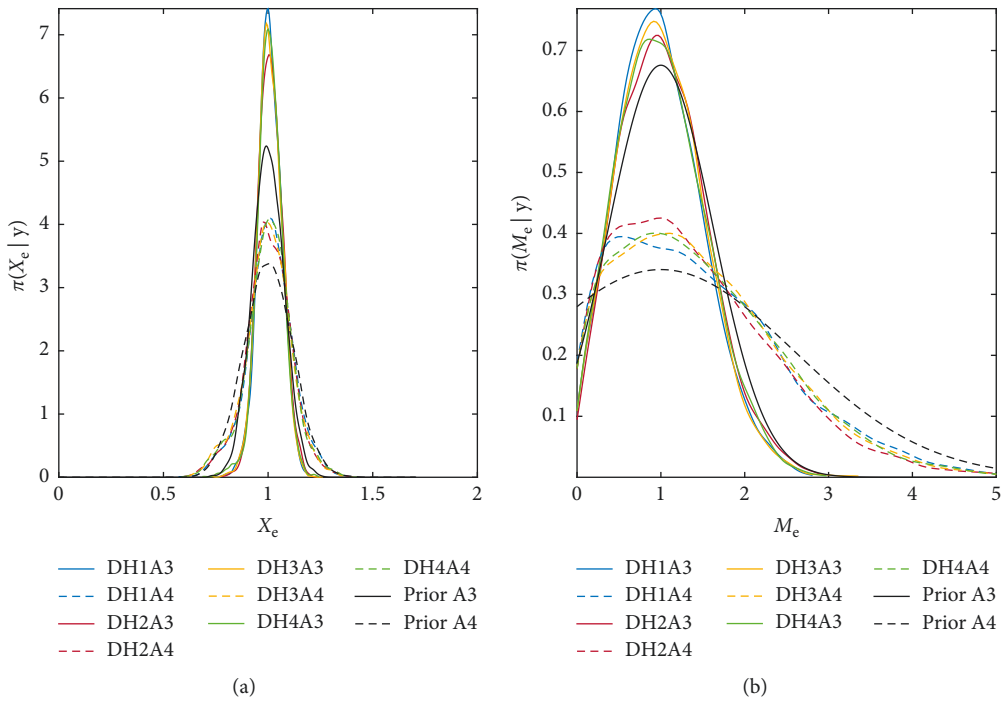

Figure 10: Anomaly scenarios A3 and A4. Prior covariance matrix with $\lambda = 5$. $X_e = (X_m/X_{true})$ and $M_e = (M_m/M_{true})$.

Table 4: Mean and standard deviation of priors $\pi_{PR}(X_m)$ and $\pi_{PR}(M_m)$ (X_m (mm) and M_m (g)).

Statistic	A1		A2		A3		A4	
	X_m	M_m	X_m	M_m	X_m	M_m	X_m	M_m
Covariance matrix with $\lambda = 2$								
Mean	298	153	300	49	861	94	859	39
Deviation	38	60	21	18	26	24	40	24
Covariance matrix with $\lambda = 5$								
Mean	298	153	300	49	861	94	859	39
Deviation	94	150	52	45	66	59	100	59

Table 5: Mean and standard deviation of marginal posteriors $\pi(X_m \mid \mathbf{y})$ and $\pi(M_m \mid \mathbf{y})$ (X_m (mm) and M_m (g)).

Statistic	A1		A2		A3		A4	
	X_m	M_m	X_m	M_m	X_m	M_m	X_m	M_m
Mean	298	153	300	49	861	94	859	39
Deviation	32	55	22	18	30	24	45	21

up to DH4A3, which are shown with continuous lines, provided approximately the same pdf. Analogous behavior occurs to the inference of scenarios DH1A4 up to DH4A4, presented with dashed lines in the same figure. Moreover, the probabilistic predictions seem to be independent on the damping model because all marginals $\pi(M_m \mid \mathbf{y})$ and $\pi(X_m \mid \mathbf{y})$ were quite similar for a specific structural anomaly. These results should bring up the discussion of how relevant are the damping models on identification strategies considered for structures which possess damping rates less than 1%. For the cases analyzed all four damping models provided similar results. This suggests that, in some situations, one could possibly adopt the most simple damping hypothesis at least for the first run of the identification algorithms. Depending on the results that are achieved, the user could make a decision concerning the need for improving the damping model. It is important to remark that these conclusions were achieved for the present structural system considering a particular experimental measurement system.

Beyond demonstrating the independence of probabilistic predictions in relation to damping models, these computational predictions show that there are expressive variations of M_m inference when scenarios A1 and A2 are compared with A3 and A4. Figure 7 illustrates that the estimations of anomaly scenarios A1 ($X_m = 300$ mm, $M_m = 158.4$ g) and A2 ($X_m = 300$ mm, $M_m = 49.6$ g) led to posterior pdfs that are approximately the same. In this case, the computational model seems not be able to differentiate a great reduction on punctual mass magnitudes. On the other hand, Figure 10 demonstrates different levels of uncertainties on estimates of A3 ($X_m = 859$ mm and $M_m = 94.5$ g) and A4 ($X_m = 859$ mm and $M_m = 36.9$ g) configurations. In the last two configurations, i.e., A3 and A4, the computational model could encode the influence of its magnitudes on system dynamic behavior in their pdfs.

Finally, the samples drawn from the posterior $\pi(\boldsymbol{\theta} \mid \mathbf{y})$ are used to compute model predictions for the FRF of the system and these are compared with their measured counterparts. Figures 11 and 12 detail the FRFs, estimated at accelerometer AC1, for configurations A1 and A4,

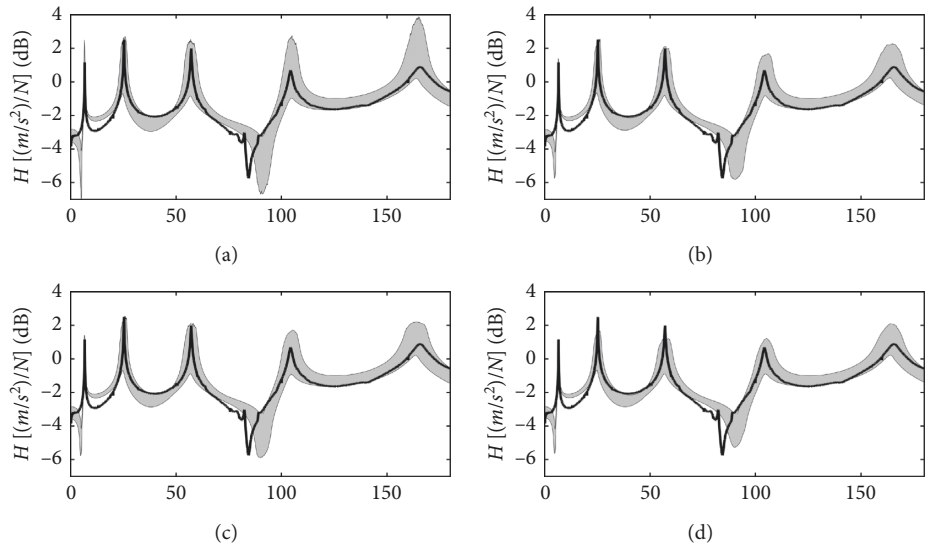

Figure 11: FRFs for scenario A1 and prior covariance matrix with $\lambda = 5$. Black continuous line: experimental FRF; greyed region: 90% credibility interval provided by model predictions. (a) Freq. (Hz) DH1. (b) Freq. (Hz) DH2. (c) Freq. (Hz) DH3. (d) Freq. (Hz) DH4.

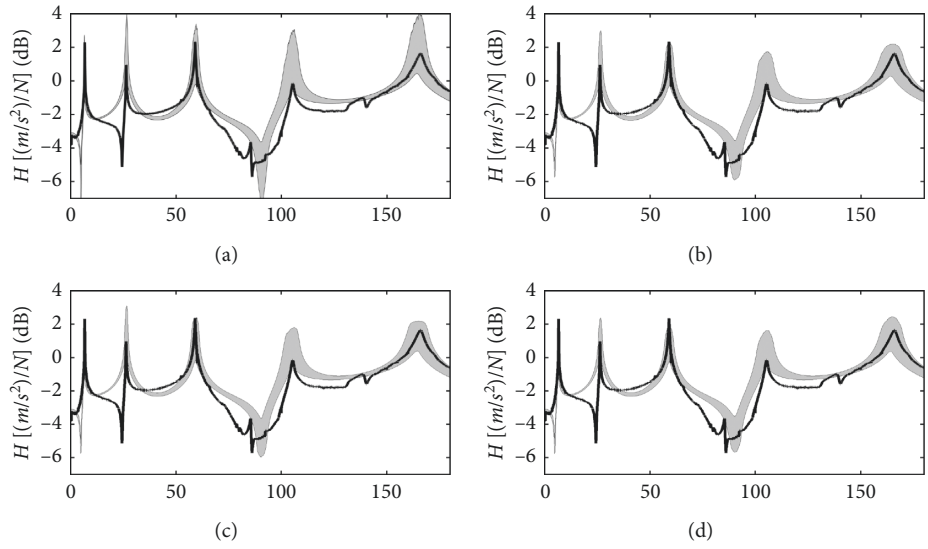

Figure 12: FRFs for scenario A4 and prior covariance matrix with $\lambda = 5$. Black continuous line: experimental FRF; greyed region: 90% credibility interval provided by model predictions. (a) Freq. (Hz) DH1. (b) Freq. (Hz) DH2. (c) Freq. (Hz) DH3. (d) Freq. (Hz) DH4.

respectively, shown in Figure 4. These two specific cases were selected because they represent the structural anomaly scenarios which have the greater and the lower magnitude of punctual masses adopted in this paper. The graphs compare the computational prediction with their measured counterparts. Firstly, it can be seen that all experimental FRF data are within the 90% confidence range of the probabilistic model. These results indicate good compliance of the computational model with the dynamical behavior of the physical system. Secondly, except for DH1 FRFs, which have the greatest amplitude resonance picks because the system was undamped, one can see that the 90% confidence range of all the remaining models DH2, DH3, and DH4 produce quite similar credibility intervals.

6. Conclusions

This paper presents an approach for damage identification of structural anomalies based on a Bayesian framework. The impact of a set of damping models on the identification results is analyzed. The exploration of posterior probability distributions of model parameters is performed by means of the Markov chain Monte Carlo method using the Delayed Rejection Adaptive Metropolis (DRAM) algorithm.

Measured data from modal analyses of an aluminum beam are considered as input data. Damage scenarios are physically simulated by placing rigid blocks over an elastic beam, and four damping models are considered in order to evaluate the impact of damping hypotheses on system

identification. The proposed model updating is quite general and can be used in other types of experimental setups for calibration, identification, and sensitivity analyses.

The main conclusions of this work are (1) the damping models provided basically the same characteristics of the posterior densities for all anomaly scenarios that were analyzed here and (2) the position X_m of the rigid blocks presented a lower level of uncertainty when compared with its mass magnitude M_m.

Data Availability

The data used to support the findings of this study are included within the article.

Conflicts of Interest

The authors declare that they have no conflicts of interest.

Acknowledgments

The authors express their gratitude to the Laboratory of Structural Dynamics and Images and Signal Processing (LADEPIS) situated on Structures and Materials Laboratory complex LABEST from civil engineering program of COPPE. This study was financially supported in part by the Coordenação de Aperfeiçoamento de Pessoal de Nível Superior-Brasil (CAPES)-Finance Code 001.

References

[1] R. Aster, B. Borchers, and C. Thurber, *Parameter Estimation and Inverse Problems*, Academic Press, Cambridge, MA, USA, 1st edition, 2004.

[2] J. E. Mottershead and M. I. Friswell, "Model updating in structural dynamics: a survey," *Journal of Sound and Vibration*, vol. 167, no. 2, pp. 347–375, 1993.

[3] E. Simoen, G. De Roeck, and G. Lombaert, "Dealing with uncertainty in model updating for damage assessment: a review," *Mechanical Systems and Signal Processing*, vol. 56-57, pp. 123–149, 2015.

[4] T. Bayes, "An essay towards solving a problem in the doctrine of chances," *Philosofical Transactions of the Royal Society*, vol. 53, pp. 370–418, 1763.

[5] R. C. Smith, *Uncertainty Quantification–Theory, Implementation and Applications*, Siam, Hillsborough Street Raleigh, NC, USA, 2014.

[6] Y. Huang, C. Shao, B. Wu, J. L. Beck, and H. Li, "State-of-the-art review on Bayesian inference in structural system identification and damage assessment," *Advances in Structural Engineering*, vol. 22, no. 6, pp. 1329–1351, 2018.

[7] L. S. Katafygiotis and J. L. Beck, "Updating models and their uncertainties. ii: model identifiability," *Journal of Engineering Mechanics*, vol. 124, no. 4, pp. 463–467, 1998.

[8] J. L. Beck, "Bayesian system identification based on probability logic," *Structural Control and Health Monitoring*, vol. 17, no. 7, pp. 825–847, 2010.

[9] W. K. Hastings, "Monte Carlo sampling methods using Markov chains and their applications," *Biometrika*, vol. 57, no. 1, pp. 97–109, 1970.

[10] N. Metropolis, A. W. Rosenbluth, M. N. Rosenbluth, A. H. Teller, and E. Teller, "Equation of state calculations by fast computing machines," *Journal of Chemical Physics*, vol. 21, no. 6, pp. 1087–1092, 1953.

[11] N. Metropolis and S. Ulam, "The Monte Carlo method," *Journal of the American Statistical Association*, vol. 44, no. 247, pp. 335–341, 1949.

[12] G. E. P. Box and G. C. Tiao, *Bayesian Inference in Statistical Analysis*, Addison-Wesley, Boston, MA, USA, 1973.

[13] E. T. Jaynes, *Probability Theory. The Logic of Science*, Cambridge University Press, Cambridge, UK, 2003.

[14] J. P. Kaipio and E. Somersalo, *Statistical and Computational Inverse Problems, Applied Mathematical Sciences*, Springer, New York, NY, USA, 1st edition, 2005.

[15] A. Tarantola, *Inverse Problem Theory and Methods for Model Parameter Estimation*, Siam, Philadelphia, PA, USA, 2005.

[16] C. R. Farrar and K. Worden, "An introduction to structural health monitoring," *Philosophical Transactions of the Royal Society A*, vol. 365, no. 1851, pp. 303–315, 2006.

[17] A. P. Bovsunovsky and C. Surace, "Considerations regarding superharmonic vibrations of a cracked beam and the variation in damping caused by the presence of the crack," *Journal of Sound and Vibration*, vol. 288, no. 4-5, pp. 865–886, 2005.

[18] R. Chandra, S. P. Singh, and K. Gupta, "Damping studies in fiber-reinforced composites–a review," *Composite Structures*, vol. 46, no. 1, pp. 41–51, 1999.

[19] R. Chandra, S. P. Singh, and K. Gupta, "A study of damping in fiber-reinforced composites," *Journal of Sound and Vibration*, vol. 262, no. 3, pp. 475–496, 2003.

[20] R. F. Gibson and R. Plunkett, "Dynamic mechanical behavior of fiber-reinforced composites: measurement and analysis," *Journal of Composite Materials*, vol. 10, no. 4, pp. 325–341, 1976.

[21] X. Ling and A. Haldar, "Element level system identification with unknown input with Rayleigh damping," *Journal of Engineering Mechanics*, vol. 130, no. 8, pp. 877–885, 2004.

[22] H. Haario, M. Laine, A. Mira, and E. Saksman, "Dram: efficient adaptive mcmc," *Statistics and Computing*, vol. 16, no. 4, pp. 339–354, 2006.

[23] R. W. Clough and J. Penzien, *Dynamics of Structures*, Computers and Structures, Inc., Berkeley, CA, USA, 3rd edition, 1995.

[24] M. Géradin and D. J. Rixen, *Mechanical Vibrations, Theory and Application to Structural Dynamics*, John Wiley and Sons Ltd., Chichester, UK, 3rd edition, 2015.

[25] M. L. M. Souza, D. A. Castello, and N. Roitman, "Model updating and uncertainty evaluation on a simply supported beam," in *Proceedings of the ICVRAM ISUMA UNCERTAINTIES 2018*, ASCE, Florianópolis, Brazil, April 2018.

[26] M. S. Cao, G. G. Sha, Y. F. Gao, and W. Ostachowicz, "Structural damage identification using damping: a compendium of uses and features," *Smart Materials and Structures*, vol. 26, no. 4, pp. 1–14, 2017.

[27] D. Gamerman and H. F. Lopes, *Markov Chain Monte Carlo*, Chapman and Hall/CRC, New York, NY, USA, 2nd edition, 2006.

[28] S. Geman and D. Geman, "Stochastic relaxation, gibbs distributions, and the Bayesian restoration of images," *IEEE Transactions on Pattern Analysis and Machine Intelligence*, vol. PAMI-6, no. 6, pp. 721–741, 1984.

[29] J. Geweke, "Evaluating the accuracy of sampling-based approaches to calculating posterior moments," Federal Reserve Bank of Minneapolis Research Department Staff, Minneapolis, MN, USA, Report 148, 1991.

[30] A. Gelman, J. B. Carlin, H. S. Stern, D. B. Dunson, A. Vehtari, and D. B. Rubin, *Bayesian Data Analysis*, Chapman and Hall/CRC, New York, NY, USA, 3rd edition, 2013.